Refereed Proceedings

Heat Exchanger Fouling and Cleaning: Fundamentals and Applications

Engineering Conferences International *Year* 2003

Sodium Aluminosilicate Solid Phase Specific Fouling Behaviour

Jonas Addai-Mensah*

Jun Li†

Marek Zbik‡

Scott Rosencrance**

*University of South Australia

†University of South Australia

‡University of South Australia

**Westinghouse Savannah River Company

SODIUM ALUMINOSILICATE SOLID PHASE SPECIFIC FOULING BEHAVIOUR

Jonas Addai-Mensah[*] [1], Jun Li[1], Marek Zbik[1] and Scott Rosencrance[2]
[1]Ian Wark Research Institute, University Of South Australia. Mawson Lakes, Adelaide. 5095 Australia.
[2]Westinghouse Savannah River Company, Aiken, SC. USA.

*Corresponding Author: Jonas.addai-mensah@unisa.edu.au; Phone: +61-8-83023673, Fax: +61-8-83023683

Abstract

Process heat transfer equipment fouling due to sodium aluminosilicate precipitation is a serious problem that confronts high-level nuclear waste liquor and Bayer process alumina processing plants. The fouling of 316 stainless steel substrate by thermodynamically stable and unstable sodium aluminosilicate polytypes: amorphous solid, zeolite A, sodalite and cancrinite crystals, been has studied in an isothermal, batch precipitation system at 65 °C.

Fouling invariably occurred via heterogeneous nucleation, crystal growth and particulate adsorption processes, accompanied by solution-mediated, phase transformation and morphological changes. For the thermodynamically stable cancrinite fouling, the amount of scale deposited increased systematically with increasing crystallization time before levelling off as a result of depleted supersaturation. Where the deposited scale involved a less stable phase (e.g., amorphous, zeolite A), transformation to a more stable phases (e.g., sodalite/cancrinite) occurred. The scale layer coverage/growth characteristically increased and then decreased in a periodic manner. The periodicity of this unusual behaviour appeared to be directly and kinetically related to polytypic phase transformation of amorphous to zeolite A, zeolite A to sodalite and sodalite to cancrinite.

Introduction

Fouling of heat transfer equipment, which occurs as a result of sodium aluminosilicate (SAS) precipitation from supersaturated sodium aluminosilicate liquors, poses an intractable scientific and technological challenge to high level nuclear waste (HLNW) liquor processing and alumina refining plants.

In a HLNW plants, high ionic strength (6 - 8 M) liquors comprising sodium, hydroxide, aluminate, nitrate, nitrate, silica and trace uranyl species are concentrated by evaporation at temperature range 30 - 140 °C. As the species concentrations increase upon evaporation, the liquor invariably becomes supersaturated with respect to sodium aluminosilicate and diuranate scale forming species. The increase in supersaturation of the sodium aluminosilicate species specifically originates from the fact that the solubility of SiO_2-containing species in the evaporator caustic aluminate liquor decreases with increasing ionic strength of dissolved Al(III) in Al(III) to NaOH molar ratio range 0.0 – 0.2. At sufficiently high supersaturations and heat fluxes, the precipitation of SAS and, sometimes, the co-precipitation of radioactive sodium diuranate particles occur. The accumulation of radionuclide scale considerably exacerbates the fouling problem and raises a serious risk issue.

In the Bayer process, Al(III)-containing mineral phases, gibbsite (γ-$Al(OH)_3$) and boehmite (AlOOH) are extracted from bauxite ores using concentrated NaOH solution at 140 – 250 ºC. At these elevated temperatures, increased dissolution of SiO_2-bearing minerals in the ore, such as quartz and kaolin, also occurs. Following ore digestion, suspension cooling and clarification, gibbsite is crystallized from Al(III)-supersaturated sodium aluminate liquors (pregnant Bayer liquor) at 60 – 90 ºC. The resulting "spent" liquor is then reheated via a series of heat exchangers for recycling and further bauxite digestion. The equilibrium SiO_2 solubility in Bayer liquors decreases with decreasing Al(III) concentration in [Al(III)]/[NaOH] molar ratio range 0.2 - 0.7. Therefore, SiO_2-contaning Bayer spent liquors are characteristically supersaturated with respect to NAS solid phases. Consequently, SAS precipitation fouling from the spent liquor, significantly facilitated by the intensity of heat prevailing in shell and tube heat exchangers, results at the steel heat transfer surfaces [Cresswell, 84; O'Neill, 86].

SAS fouling management requires very costly handling methods and treatment approaches. First and foremost, foulant deposition significantly reduces heat exchanger efficiency with a significant, adverse impact on production, labour and maintenance costs. In HLNW processing plants, uncontrolled fouling by radioactive solids may occur at an alarming rate and pose a major criticality concern, warranting complete plant shutdown. Effective management and mitigation of sodium aluminosilicate fouling in process heat transfer equipment are, therefore, of significant importance to industry. Increased research effort and initiatives with multi-disciplinary approach are required for achieving an expeditious mitigation solution.

The main sodium aluminosilicate phases that foul process heat exchangers or evaporators used in handling caustic aluminosilicate liquors may comprise amorphous solid, zeolite A, sodalite and cancrinite crystals. The amorphous solid is the least thermodynamically stable phase and kinetically pre-disposed to form first,

particularly at low temperatures (< 85 ^{o}C) [Barnes et al., 1999a and b]. It rapidly transforms into zeolite A which, in turn, readily transforms into sodalite with time [Gerson et al. 1996, Barnes et al., 1999a & b]. Upon further aging, sodalite undergoes a dimorphic phase transformation to cancrinite over several hours. The mechanism and kinetics of SAS precipitation and phase transformations have been investigated under a variety of conditions [Addai-Mensah et al., 1997; Addai-Mensah et al., 1998 Barnes et al., 1998; Barnes et al., 1999a-d; Gerson and Zheng, 1997].

The fouling behaviour and crystal growth kinetics of pure sodalite and cancrinite phases and their dimorphic mixtures in synthetic, sodium aluminosilicate liquors have been studied under isothermal, batch precipitation conditions [Barnes et al., 1998; Barnes et al., 1999a-e]. The desilication mechanism, leading to scale formation from optically clear liquors at moderate supersaturations, involved substrate-mediated heterogeneous nucleation and crystal growth. For sodalite crystal/scale layer growth, an activation energy of 30 kJ mol^{-1} and a second order dependence of the desilication rate upon relative supersaturation of SiO_2 were reported. For cancrinite, the crystal growth rate was dependent upon SiO_2 relative supersaturation to the power of 3 with an activation energy of 80 kJ mol^{-1}. The phase transformation rate strongly increases with increasing temperature. The mechanism is solution-mediated, with the dissolution of the less stable phase and concomitant heterogeneous nucleation and growth of a more stable phase.

As a method of sodium aluminosilicate fouling mitigation, sodalite and cancrinite seeding of SiO_2-supersaturated caustic aluminate liquors has been studied. NAS seeding resulted in rapid desilication, accompanied by remarkable suppression of scale formation on steel substrates [Gerson et al., 1998; Barnes et al. 1998; Barnes et al. 1999d]. Whilst several reported studies have considerably advanced our knowledge and understanding of sodium aluminosilicate fouling behaviour, there is still a considerable paucity of knowledge of the influence of polymorphism and solid phase transformation on the nature and extent of scale layer growth. For example, solid phase dependent fouling behaviour and evolution of scale layer with crystallization time are as yet not fully investigated. Given 2 solid phases, where one is stable (e.g., cancrinite) and the other unstable (e.g., amorphous), it is unclear as to how the nature and evolution of the scale layer deposited on steel substrate with time relates to their crystallo-chemical structures of the phases. The main focus of the present work is to investigate thermodynamically stable (cancrinite) unstable and metastable (amorphous zeolite A and sodalite,) SAS phase specific fouling behaviour at stainless steel substrates surfaces under industrially relevant heat transfer and solution conditions. This was achieved through isothermal batch crystallization studies carried out at 65 ^{o}C using unseeded and seeded, synthetic, supersaturated caustic aluminosilicate liquors.

Methodology

Isothermal, batch desilication experiments using synthetic optically clear sodium aluminosilicate liquors were conducted in a stirred (400 rpm), well-sealed 2.5 dm^3, baffled crystallizer. A thermostatically controlled oil bath provided a constant temperature to within 0.1 ^{o}C. A 4-blade, 45 ^{o}-pitch impeller which provided agitation was modified to allow screw attachment of three, 1.5 × 2.0 cm, 316 stainless steel coupons (Figure 1) at 45 ^{o}-pitch to the impeller shaft and 4.0 cm from the bottom of the shaft. A further 24 stainless steel coupons were attached 90 ^{o} to 4 baffles attached the crystallizer wall. Before their use, each coupon was marked at 3 different areas (Figure 1: A, B, and C) so that identical positions on different coupons could be microscopically analysed. This procedure was found to be necessary due to the inherent variation in scale layer structure and thickness across the length of the tokens which results from the differences in local normal and Reynolds shear stresses and turbulence [Pettersson and Rasmuson, 1998]. Analysing similar areas significantly reduced the hydrodynamically induced variability in scale layer features. Slurry and fouled substrate samples were periodically (e.g. 3, 5, 15, 30, 60, 120 and 240 min) removed for solids characterization and solution assay. Filtrate solutions were analysed for SiO_2 and Al(III) concentrations by Inductively Coupled Plasma (ICP) spectroscopy (Spectro Analytical Instruments, Spectro SIM-SEQ ICP-OES, Kleve, Germany) by pipetting 2 cm^3 of the sample in to 10 cm^3 of approximately 20% HCl solution and then diluting to 250 cm^3. The relative error in SiO_2 analysis was determined to be < 3 %.

For solid phase analysis, steel tokens detached from the impeller shaft and baffles and filtered suspension solids were washed in Milli-Q water until they were free from alkali, before desiccation. The three marked areas (A, B and C) were analysed at magnifications of 250, 500, 1000, and 2000 times by scanning electron microscope (SEM) in both backscattered electron (BE) and secondary electron (SE) imaging modes to determine the extent of scale coverage, crystal size and morphology. The extent of surface coverage by sodium aluminosilicate scale was estimated from SEM photomicrographs by the image analysis program STIMAN provided by Moscow State University (Sergeev et al., 1983a & b). The STIMAN analysis provided a statistical analysis and measure of foulant surface coverage and scale particle size distribution in the form of various parameters: specific area, particle perimeters and equivalent diameters. It involved images captured at several (e.g., 5) magnifications in the range 2000 - 100000), revealing variations in structural elements of samples over a broad size scale (nanometres up to millimetres). SEM imaging and energy dispersion spectroscopy (EDX) analysis of carbon-coated samples was achieved using a high resolution field emission Cam Scan (CS44FF, Cambridge, UK) at 15 kV. For solid/crystalline phase crystallographic analysis, x-ray powder diffraction (XRD, Phillips PW1130/90) was used. The XRD patterns were collected

on powdered samples in 2θ scanning mode using CuKα radiation (λ = 1.5418 Å).

Sodium aluminosilicate liquors were prepared from high purity gibbsite (C-31 Hydrate, Alcoa Arkansas, USA) and sodium hydroxide (99 % pure, 1.0% Na_2CO_3, Ajax Chemicals, Australia), sodium metasilicate (99 % pure Ajax Chemicals, Australia), Analytical reagent (AR) grade sodium nitrate (99 % pure, Ajax Chemicals, Australia), AR grade sodium nitrite (99 % pure, Ajax Chemicals, Australia) and Milli-Q water (surface tension of 72.8 mN m^{-1} at 20°C and a specific conductivity <0.5 μS).

The test liquor was made by mixing equal volumes of nitrate/nitrite-rich sodium aluminate (4.00 M NaOH, 2.00 M $NaNO_3$, 2.00 M $NaNO_2$ and 0.376 M Al(III)) and sodium metasilicate (4.00 M NaOH and 0.35 M SiO_2) solutions. Thus, the resulting sodium aluminosilicate solution species concentrations (C) were: 4.00 M NaOH, 1.00 M $NaNO_3$, 1.00 M $NaNO_2$, 0.175M SiO_2, 0.188 M Al(III). Due to the significantly different equilibrium solubilities of the 4 SAS phases, with the amorphous being the most soluble phase whilst cancrinite was the least soluble [Barnes et al., 199c; Zheng et al. 1997& 1998], the initial relative supersaturation (σ = C/Ce- 1) for the 4 phases were accordingly different. For the above solution composition, the initial SiO_2 and Al(III) σ ranged from 0.5, based upon the amorphous phase, to 69 (SiO_2) and 32 (Al(III)), both for the cancrinite phase. To prepare a sodium aluminate solution, the required mass of sodium hydroxide was added to 50 % of the total volume of water required in a stainless steel beaker. After complete dissolution, a known mass of aluminium hydroxide was added. The mixture was then heated to 105 °C. After complete dissolution, known masses of sodium nitrate and nitrite and water were added to make up the required liquor volume and ionic strength. The sodium metasilicate solution was similarly prepared from known masses of sodium hydroxide and sodium metasilicate.

To run an experiment, the crystallizer was first charged with 1.15 dm^3 of sodium aluminate solution. The vessel was then sealed and heated to 65 °C at an agitation rate of 400 rpm. This agitation rate together with the prevailing solution kinematic viscosity and impeller diameter provided strong axial mixing. Once the temperature had equilibrated at 65 °C, 1.15 dm^3 of sodium silicate solution preheated to 65 °C was gradually added (to avoid local over-supersaturation) to the crystallizer to give a final solution volume of approximately 2.3 dm^3.

In seeded experiments, a predetermined quantity sodium aluminosilicate seeds were added and the experimental time was subsequently set as zero as soon as the temperature equilibrated at 65 °C. Experiments with each solid phase were repeated at least six times over a crystallization time of 75 h. The seeds were prepared by unseeded precipitation performed over different times to allow the recovery of the individual, distinct SAS phases. Particle size analysis by laser diffraction showed the seed particle size to be ~ 0.8 to 10 μm. A 5-point N_2 BET method was used to determine porosity and surface area of seed/scale particles.

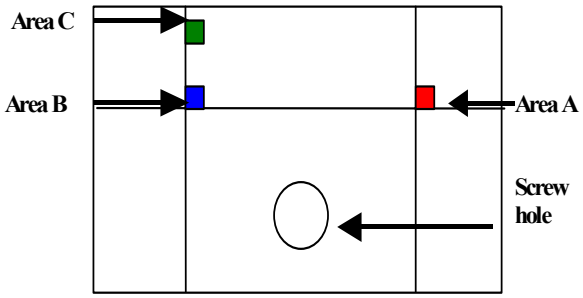

Figure 1: Stainless steel coupon showing marked areas for reproducible SEM imaging and fouling analysis.

Results and Discussions

SEM secondary electron images (Figure 2) used for providing morphological information were observed not to suitable for quantitative image analysis. To enhance the contrast between the aluminosilicate particles and the steel substrate, the images were collected in BE mode, in which the sodium aluminosilicate crystals appear in regions of dark contrast on the bright background of the stainless steel substrate (Figure 2B). Such BE images facilitated accurate quantitative STIMAN image analysis.

Cancrinite-seeded fouling behaviour

The cancrinite seeded fouling experiment was performed first to provide benchmarking information from a thermodynamically stable system of which fouling proceeded with no phase transformation complexities. The behaviour of such a stable foulant enabled accurate comparison with those of the less stable solid phases (amorphous, zeolite and sodalite). The seed particles ranged from 0.6 to 3 μm in size. The fouling behaviour of steel tokens removed from cancrinite-seeded sodium aluminosilicate solution (initial seed charge = 5.28 g cm^{-3} or 239.4 m^2dm^{-3}) at 65 °C is shown Figures 3 and 4.

The SEM photomicrographs showed that highly colloidal size particles proliferated the steel substrate surfaces almost instantaneously (within 3 min of crystallization) (Figures 3 and 4). The particles deposited initially are approximately 100 – 200 nm in size and thus, are much smaller than the original seed particles. Complementary dynamic light scattering analysis of unseeded solution samples showed that within the first 5 min of crystallization, SAS particles of sizes > 20 nm were not present in the bulk solution which was optically clear. The lack of a detectable amount of colloidal SAS particles in bulk solution indicate that, the 100 – 200 nm scale particles observed initially formed as a result substrate-mediated heterogeneous and secondary nucleation and particle growth processes. This observation is consistent with mechanism of SAS scale

formation reported in previous studies [Addai-Mensah et al., 1997 & 1998).

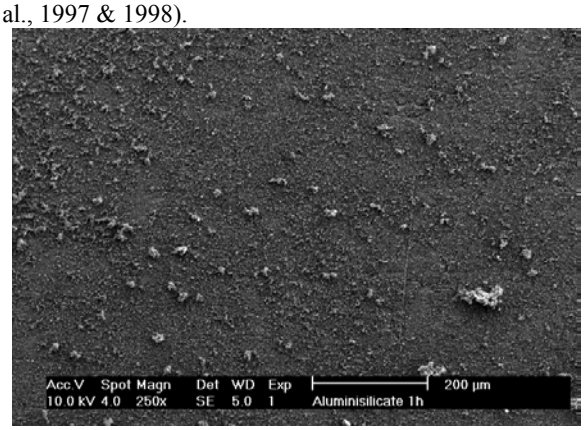

A

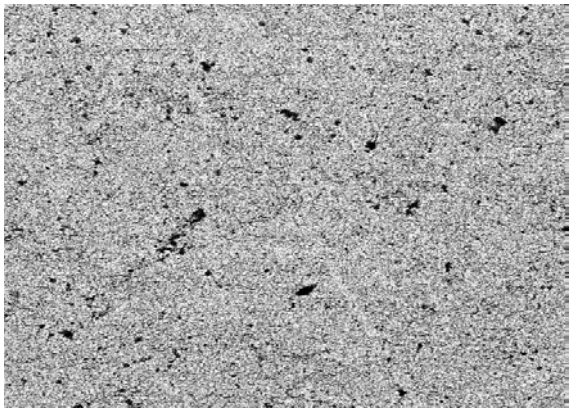

B

Figure 2 SEM micrograph of fouled 316 stainless steel substrate in SE (**A**) and BSE (**B**) modes at 250 magnification produced from cancrinite-seeded sodium aluminosilicate solution at 65^{o}C and after 1 h.

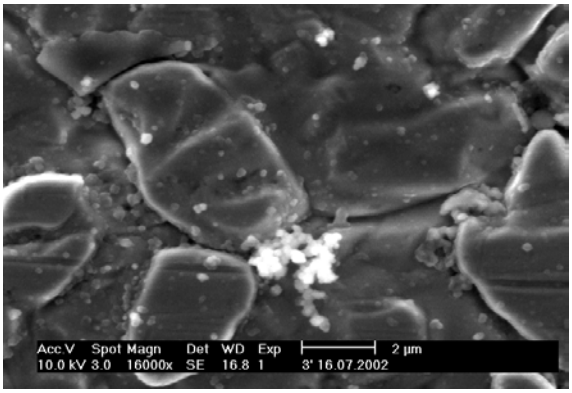

A

Figure 3: Secondary electron micrograph of 316 stainless steel coupon fouled with colloidal size crystals after 3 min cancrinite-seeded crystallization at 65 ^{o}C.

Nucleation in the bulk solution occurred, as colloidal particles were noticeably present in the samples removed periodically from the crystallizer. The amount of scale deposited at the steel substrate surfaces increased markedly with increasing crystallization time, being more rapid over the first 90 min. Well rounded primary scale-forming particles were observed. The individual grains increased systematically in size with time due to pure crystal growth. Furthermore, some of the parent (seed) crystals were deposited at the steel substrate surface by a particulate fouling mechanism, as shown at the bottom of SEM image in Figure 4 (A).

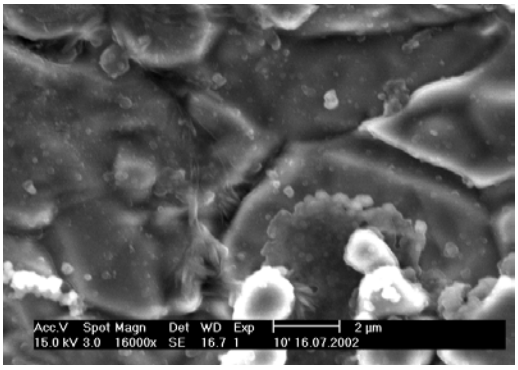

A

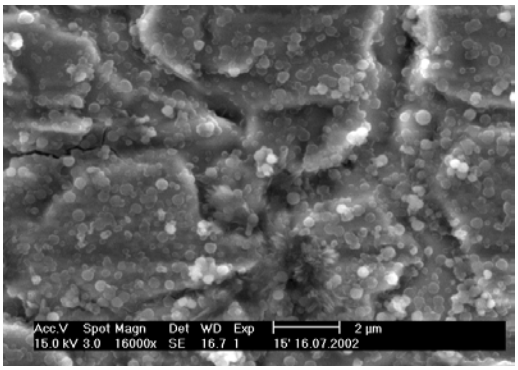

B

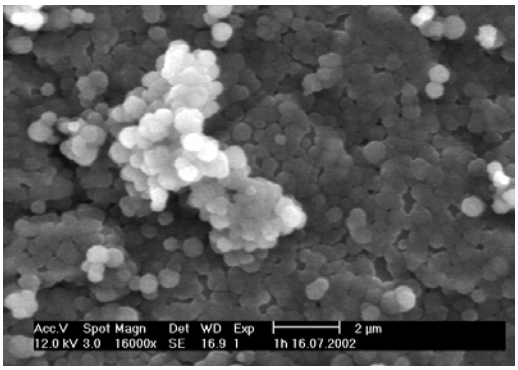

C

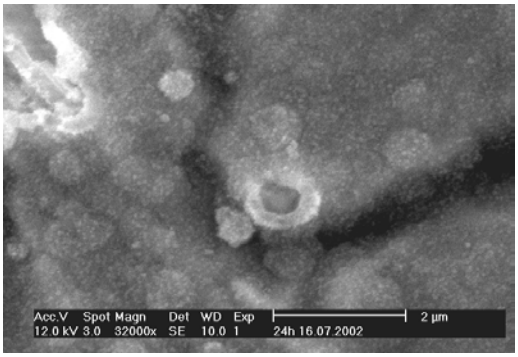

D

Figure 4: Secondary electron micrograph of 316 stainless steel substrate fouled with cancrinite crystals

after: 10 min (**A**), 15 min (**B**), 1 h (**C**) and 24 h (**D**) of cancrinite-seeded crystallization at 65 ^{o}C.

Subsequent STIMAN analysis revealed that the relative particle area increased from about 13 % to more than 70 % after 60 min. As shown in Figure 5, the scale coverage steadily increased to ~ 93 % the total surface area of the steel coupon in the first 90 min of crystallization, before levelling off thereafter.

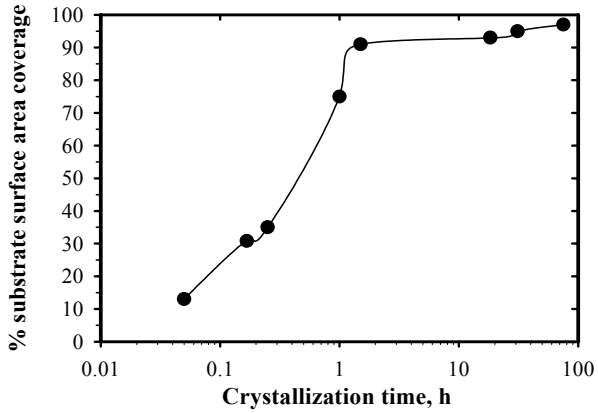

Figure 5: Extent of steel substrate fouling as function of time produced from cancrinite-seeded sodium aluminosilicate solution (NaOH = 4M, $NaNO_3$ = 1M, $NaNO_2$= 1M, initial SiO_2 = 0.175M, Al(III) = 0.188M and initial seed charge = 5.28 g cm^{-3} = 239.4 m^2dm^{-3}) at 65 ^{o} C. XRD analysis confirmed the scale product as cancrinite throughout the fouling process.

Amorphous phase-seeded fouling behaviour

The fouling behaviour of steel coupons removed from the suspensions seeded with 0.3 – 3 µm amorphous particles (seed charge = 5.28 g cm^{-3} = 239.4 m^2dm^{-3}) at 65 ^{o} C is shown in Figure 6. SEM examination indicated that the fouling occurred almost instantaneously via heterogeneous/secondary nucleation and particulate deposition with a steady increase in scale layer coverage over the first 30 min before increasing rapidly thereafter (Figure 6(A-D)). The primary scale particles deposited after 3 min were globular in shape and ≈100 – 200 nm in size. The scale particles grew into 500-600 nm sizes within 1 h. The presence of voids, indicating a partial steel substrate surface coverage, was still evident after 1 h. Upon further aging (up to 6 h), there was a small but noticeable decrease in size the average particle and a marked increase in the voids, as exhibited in Figure 7 (A) for a coupon fouled after 6 h. The particles formed after 50 h were intergrowth of elongated, 100 nm particles. Selected area EDX analysis confirmed the voids to be substantially NAS particulate-free.

STIMAN image analysis of the fouled coupons showed that an increase in scale coverage of ≈ 75 % steel surface occurred within the first 1 h. Upon further aging, the scale coverage decreased with time over several minutes and then increased again to maximum (Figure 8). After 31 h, the average surface area coverage decreased and then increased steadily. The average scale particle diameter and perimeter displayed similar "sinusoidal" trend over a 75 h period (Figure 8).

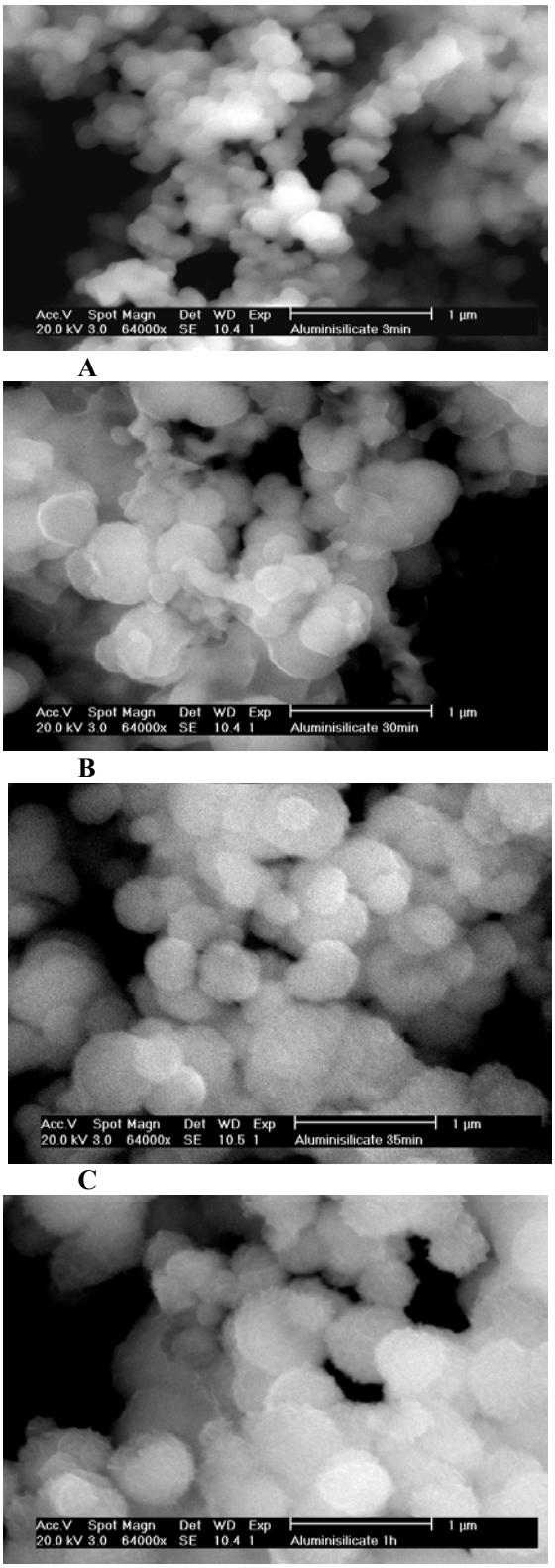

Figure 6: SE micrograph of fouled steel substrate fouled after: 3 min (**A**), 30 min (**B**) 35 min (**C**) and (**C**) 1 h of amorphous-seeded crystallization at 65 ^{o}C. (NaOH = 4M, $NaNO_3$ = 1M, $NaNO_2$ = 1M, SiO_2 = 0.175M, Al(III)

= 0.188M and seed charge = 5.3 g cm^{-3} = 239.4 m^2dm^{-3}).

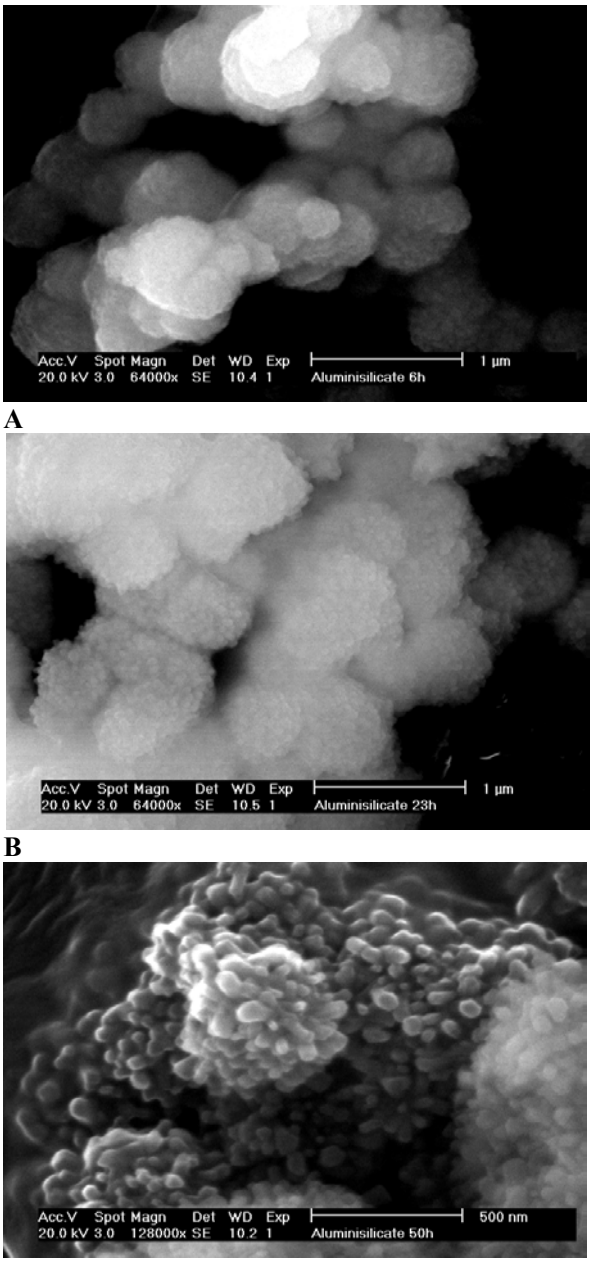

Figure 7: Secondary electron micrograph of fouled 316 stainless steel substrate with amorphous solid particles after: 6 h (**A**), 23 h (**B**) and 50 h (**C**) of amorphous-seeded crystallization at 65 ^oC.

X-ray powder diffraction analysis of all the precipitation products formed over a 75 h period was performed. Diagnostic diffraction peaks of the individual SAS phases were established for semi-quantitative identification of the mixed solid phases products [3-5].

Typical XRD analysis of the scale is exhibited in Figure 9 (A & B). The diffraction patterns show that the solid material precipitated within the first 60 min was an X-ray indifferent amorphous phase. Furthermore, zeolite A was the NAS crystalline phase formed after 3 h. Upon several hours (>30 h) of further aging, sodalite and cancrinite phases formed sequentially, as summarised below.

[Na-aluminosilicate ions]$\longrightarrow$Amorphous $\longrightarrow$ zeolite A $\longrightarrow$ Sodalite $\longrightarrow$ Cancrinite.

The amorphous and zeolite A solid phases were of similar dimorphic structures that may be described by a common formula as $Na_{11.9}Al_{12}Si_{11.5}O_{47.4}\bullet 27H_2O$. The sodalite and the cancrinite crystals displayed similar dimorphic structural characteristics that may be generically described as $Na_6\ Al_6Si_{5.9}O_{23.9}\bullet 2.0NaNO_3\bullet xH_2O$, where x is the number of moles of water of crystallization, determined to be 3.5 and 2.5 for sodalite and cancrinite, respectively.

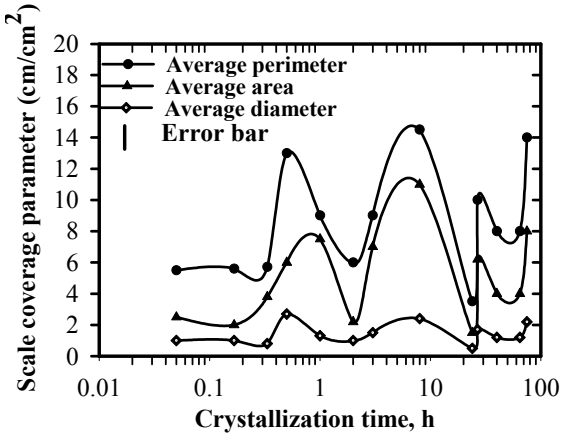

Figure 8: The evolution of estimated fractional area coverage and scale particle size with time at fouled steel substrate surfaces produced from amorphous-seeded sodium aluminosilicate solution precipitation at 65 ^oC over 75 h. Typical error bar is shown for the average surface area coverage of the NAS scale.

To further unravel the mechanism polytypic phase transformation as a part of the fouling process, a liquor at SiO_2 and Al(III) concentrations close to the amorphous solid phase equilibrium solubility 65 ^oC was seeded with bimodal particle distribution of dimorphic amorphous (fine) and zeolite A (coarse) mixed phases (1 in Figure 10). Under the amorphous phase equilibrium solubility condition, the liquor was supersaturated only with respect to zeolite A, as the latter has a much lower solubility. Hence, the amorphous solid may undergo Oswald ripening and/or phase transform to zeolite A upon aging, whilst the zeolite A crystal growth is expected with time. Figure 10, exhibiting evolution of the dimorphic, bimodal particle size distribution as function of time, shows a systematic decrease of the mass and size fraction of the amorphous phase and concomitant increase of zeolite A mass fraction. This suggests that either the dissolution or agglomeration of the amorphous phase occurred.

XRD analysis of the products confirmed that the zeolite A component in the mixed dimorphic particles increased substantially whilst the amorphous fraction showed a concomitant decrease. Thus the former crystallized at the expense of the supersaturation created by the dissolution of amorphous seed particles. This observation is consistent with the dimorphic, bimodal particle size distribution analysis (Figure 10), and enables the possibility of an agglomeration effect being the cause for the disappearance of the amorphous particles to be discounted completely.

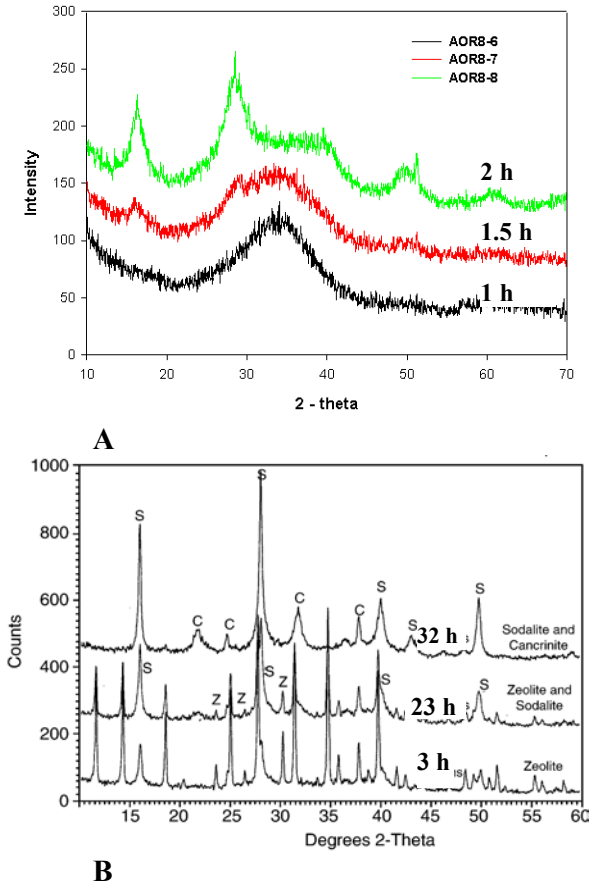

Figure 9: XRD analysis of scale formed on steel substrate during amorphous seeded precipitation at 65 °C. Phase transformation from amorphous (AOR8-6) at 1 h to zeolite A (AOR8-8) at 2 h is shown in (A), whilst zeolite A - sodalite – cancrinite transformations are exhibited in (B). Z, S and C denotes zeolite A, sodalite and cancrinite peaks, respectively.

Based on the above results, the following mechanism is proposed to rationalize the observed pattern of an increase followed by a decrease in scale layer coverage, as displayed in Figures 8. An increase in scale layer coverage is achieved under supersaturation conditions as a result of the growth in size and number deposited particles of a given solid phase with time until phase transformation starts to occur. Scale layer coverage/growth persists until at some point the supersaturation is dissipated and equilibrium solubility limit for that SAS phase is reached. Further aging beyond this point leads to transformation into the next, more metastable SAS phase, which proceeds via a dissolution and re-crystallization mechanism as shown in Figure 10 and in the manner Barnes et al. [1999b].

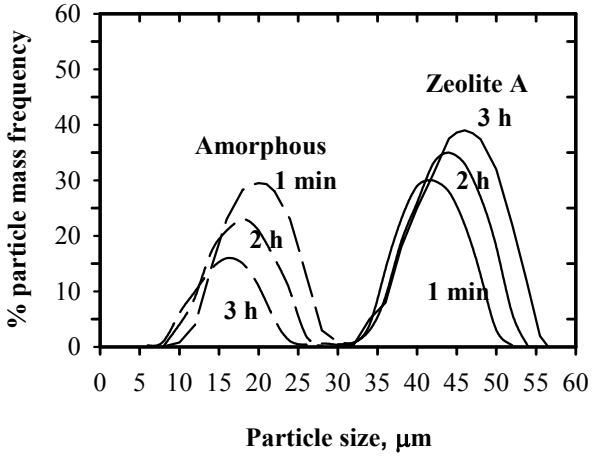

Figure 10: Evolution of dimorphic, bimodal particle size distribution as a function of aging time: 1 min (1), 2 h (2) and 3 h (3), indicating simultaneous size and mass reduction of amorphous solid particles and growth of Zeolite A crystals from sodium aluminosilicate liquor at close to amorphous phase equilibrium solubility at 65 °C.

The periodic decrease in scale coverage and polytypic phase transformation (e.g., amorphous to zeolite A) are directly linked by an associated particulate removal process. As a result of the dissolution of the cementation layer holding the less stable, globular scale particles together, particles are dislodged from the steel substrate surface by the fluid shear forces provided by agitation at 400 rpm. Where the deposit comprises a thermodynamically stable SAS phase (cancrinite), an increase in scale coverage results from continuous growth of a tenacious scale layer. In this case supersaturation is the main factor limiting in the kinetics and extent of fouling throughout the process.

Conclusions.

Studies carried out to investigate the isothermal, batch precipitation fouling behaviour of thermodynamically stable and unstable sodium aluminosilicate solid phases reveal a strong solid phase crystallo-chemical structure dependency. Quantitative SEM image analysis performed in tandem with XRD characterization of the precipitation products show that the deposition of thermodynamically stable cancrinite scale at stainless steel substrate surface systematically increased with precipitation time as expected, before levelling off to > 96 % surface area coverage after 75 h. On the other hand, where fouling involved the precipitation and transformation of less stable solid phases (e.g., amorphous and zeolite A) into more stable phases (e.g., sodalite/cancrinite), the scale

layer coverage/growth was accompanied by a periodic reduction over a 75 h period.

It appears that fundamental dissolution and re-crystallization processes, which underpin solution-mediated SAS polytypic phase transformation, play a pivotal role in the observed cycle of increase and reduction in the amount of scale deposited or its layer coverage. The periodicity of the increasing - decreasing fouling behaviour is directly linked to the mechanism and kinetics of phase transformation, which occurred sequentially as: amorphous to zeolite A, zeolite A to sodalite and sodalite to cancrinite. The findings shed more light into the mechanism of sodium aluminosilicate fouling in steel heat transfer systems where solid phase transformation is involved.

Nomenclature

C	instantaneous solution concentration of Al(III) and SiO_2 (M).
Ce	equilibrium solubility of Al(III) and SiO_2 (M).
x	water of crystallization (moles)
HLNW	High level nuclear waste
SAS	Sodium aluminosilicate
σ	relative supersaturation of Al(III) and SiO_2.

References

Addai-Mensah, J., Gerson, A.R., O'Dea, A. and Smart, R.St.C., 1997, the precipitation mechanism of sodium aluminosilicate scale in Bayer plants, *Light Metals*, 23-28.

Addai-Mensah, J., Gerson, A.R. and Smart, R. St. C., 1998, Continuous Plug Flow Precipitation of Sodalite scale on steel heat transfer surfaces, *Light Metals* 21-28.

Barnes, M.C., Addai-Mensah J. and Gerson, A.R., 1998, The Kinetics of Desilication of Synthetic Spent Bayer Liquor Seeded with Cancrinite Crystals, *J. Crystal Growth* 200, 251-264.

Barnes, M.C., Addai-Mensah J. and Gerson, A.R., 1999a, A Methodology for Quantifying Sodalite and Cancrinite Phase Mixtures and the Kinetics of the Sodalite to Cancrinite Phase Transformation, *Mesoporous and Macroporous Solids* 31 303-319.

Barnes, M.C., Addai-Mensah J. and Gerson, A.R., 1999b, the Mechanism of the Sodalite-to-Cancrinite Phase Transformation in Synthetic Spent Bayer Liquors, *J. Microporous and Mesoporous Materials* 31, 287-302.

Barnes, M.C., Addai-Mensah J., Smart, R. St. C., and Gerson, A.R., 1999c, The Solubility of SiO_2 in Synthetic Spent Bayer Liquor Seeded with Sodalite and Cancrinite, *J. Colloids and Surfaces A* 157 (1-3) 101 – 116.

Barnes, M.C., Addai-Mensah J. and Gerson, A.R., 1999d, The Kinetics of Desilication of Synthetic Spent Bayer Liquor and Sodalite Crystal Growth, *Colloids and Surfaces A* 147, 283-295.

Cresswell, P.J., 1984, Factors affecting Desilication of Bayer Process Liquors', *Proceedings of Australian Chemical Engineering Annual conference, Chemeca* 84 Paper 9c 285.

Gerson, A.R. and Zheng K., 1997, Bayer Process Plant Scale: Transformation of Sodalite to Cancrinite, *J. Crystal. Growth,* 171 209-218.

Gerson, A.R., Addai-Mensah, J., O'Dea A. and Smart, R.St.C., 1996, The Mechanism of Sodium Aluminosilicate Scale Formation in Bayer refineries, *Proceedings of the 4th International Alumina Quality Workshop, Darwin, Australia*, 393-400.

O'Neill, G.A., 1986, Prediction of Heat Exchanger-Heat Transfer Coefficient Decay due to Fouling, *Light Metals*, 133-139.

Pettersson, M. and Rasmuson, A.C., 1998, Hydrodynamics of Suspensions Agitated by Pitched-Blade Turbine, *AIChE Journal*, Vol. 44 (3) 513-527.

Roach, G.I.D, and Cornell, J.B., 1985, Scaling in Bayer plants, *Proceedings of Australian Chemical Engineering Annual conference, Chemeca 85, Paper B7A* 217.

Sergeev, Y.M., G.V. Spivak, Sasov, A.Y., Osipov, V.I. Sokolov, V.N. and Rau, E.I., 1983a, Quantitative Morphological Analysis in a SEM-Microcomputer System-I. Quantitative Shape Analysis of Single Objects, *J. Microscopy*, 135 1-12.

Sergeev, Y.M., G.V. Spivak, Sasov, A.Y., Osipov, V.I. Sokolov, V.N. and Rau, E.I., 1983b, Quantitative Morphological Analysis in a SEM-Microcomputer system-II. Morphological analysis of Complex SEM Images. *J. Microscopy*, 135 13.

Zheng, K., Gerson, A.R., Addai-Mensah J. and Smart, R. St.C., 1997, The Influence of Sodium Carbonate on Sodium Aluminosilicate crystallization and Solubility in Sodium Aluminate Solutions, *J. Crystal Growth* 171, 197-208.

Zheng, K., Smart, R. St.C., Addai-Mensah, J. and Gerson, A.R., 1998, The solubility of sodium aluminosilicates in synthetic Spent Bayer liquor, *J. Chemical and Engineering Data* 43, 312-317.

Gerson, A.R., Addai-Mensah, J., R. Smart, St.C. and Zheng, K., Sodium aluminosilicate scale control in the Bayer process, Australian Patent No PO8116/97 (1998).